Synthesis of Tin Oxide Nanoparticles (SnO_2 NPs) and its Application in the Photocatalytic Degradation of Waste Alizarin DYE

Shukra Raj Regmi[1*], Nurul Hoda Khan[1], Narendra Prakash Shawad[1], Dikpal Kumar Shahi[1], Padam Raj Joshi[1], Anup Basnet Chetry[1], Lekha Nath Khatiwada[2], Ram Prasad Baral[3], Rameshwar Adhikari[4*]

[1]Central Department of Biological and Chemical Sciences, Mid-West University, Surkhet, Nepal

[2]Department of Customs, Ministry of Finance, Kathmandu, Nepal

[3]Central Department of Chemistry, Tribhuvan University, Kirtipur, Kathmandu, Nepal

[4]Research Centre for Applied Science and Technology, Tribhuwan University, Nepal

**Correspondance: shukra.regmi@mu.edu.np / nepalpolymer@yahoo.com; Ph. 9849024059*

Keywords
SnO_2 NPs
Dye-degradation
Alizarin
Photo-light catalysis
Catalytic efficiency

Received: 13 November 2024
Revised: 5 December 2024
Accepted: 12 December 2024

ISSN: 3059 - 9687
Copyright: @Author(s) 2024

Abstract

The potential application of tin oxide nanoparticles in the photocatalytic degradation of toxic dyes has been investigated. In the present work, we have synthesized tin oxide nanoparticles by reducing tin chloride precursor, adding sodium borohydride under a controlled pH pathway. The synthesized nanoparticle was characterized by a UV-Visible Spectrophotometer, Fourier Transfer Infra-Red (FT-IR), Energy Dispersive X-ray (EDX), and X-ray Crystallography. On solving Debey-Scherrer's equation, the average size of the particle is found to be 41.28 ± 14.59 nm with a crystallinity of 85.52%. The photocatalytic degradation is achieved by the average solar radiation of 5.64 ± 0.14 kWh/m^2/day. The result reveals that complete degradation in light is obtained in 120 minutes, whereas in dark it is prolonged up to 300 minutes. The SnO_2 NPs show 100% photocatalytic efficiency in the short time frame, but dark medium catalysis was limited to 68%. The photocatalytic degradation efficiency of SnO_2 NPs is found to be superior to its catalytic degradation in the dark. The catalysis obeys pseudo-first-order kinetics with a high-rate constant. The mineralization process confirms the de-toxification of dye, which explores the application of SnO_2 NPs as a potential catalyst. Our finding claims that tin oxide nanoparticles are efficient in solar-driven photocatalytic degradation of alizarin dye in a short period.

Introduction

The nanoparticles are tiny materials having sizes varying from 1-100 nm. They show noble physical and chemical properties due to their distinguished dimensional properties (Feynman, 2018). Nanoparticles are extensively used in catalysis, drug delivery and discovery, electronic, optoelectronics applications, medical, and environmental fields (Rehan *et al.*, 2024; Stark *et al.*, 2015). Nanomaterials are unique due to their size as well as a higher surface atom-to-volume ratio in comparison to bulk material, which increases the reactivity of particles (Chen & Mao, 2007; Daniel & Astruc, 2004). Tin oxide nanoparticles are generally used in sensor technology, lithium-ion batteries, and catalysis.

The band gap of Tin oxide nanoparticles is observed between 3.6-4.00 eV depending upon the size of the particle (Din *et al.*, 2022; Khalilzadeh-Rezaie *et al.*, 2015). When the particle size decreases, the band gap increases due to the quantum confinement effect, such a tunable band gap makes SnO_2 nanoparticles the most promising semiconducting materials in photocatalytic degradation of dyes (Din *et al.*, 2022; Hardy & Aust, 1995; Lilletvedt *et al.*, 2010). Different techniques are applied to synthesize nanoparticles including Top-down and Bottom-up approach. Among the Bottom-up approach, we have synthesized SnO_2 nanoparticles by the sodium borohydride reduction method in the $SnCl_2$ precursor solution (Kader *et al.*, 2023; Kumar *et al.*, 2020). The chemical reduction method is a very sensitive approach operated by a controlled pH method. The sodium borohydride is a strong reducing agent having a standard reduction potential -1.24 V. It reduces Sn^{2+} salt into the free metal at a constant stirring of 250 rpm in a magnetic stirrer at room temperature. The obtained free tin was further muffled to get Tin oxide nanoparticles (Alcântara *et al.*, 2020; Somerville *et al.*, 2016).

Synthetic organic dyes are very toxic and even carcinogenic due to their complex structure containing aromatic amines, polyphenolic, and azo groups with organometallic bonding. Toxic metals like lead, cadmium, chromium, iron, and aluminum are embedded in dyes, their degradation ultimately accumulates in the bodies causing serious vital organ failure and carcinogenic activities. The long-term contamination and accumulation in the body may interfere the biological processes like metabolism, hormonal activity, nucleic acid synthesis, etc. (Magnavita, 2018; Sahin *et al.*, 2019; Shi *et al.*, 2016). The severe exposure of alizarin in soil or aquatic bodies may cause disturbance in the ecological cycle. Alizarin is a synthetic dye belonging to anththaloquinone having two-hydroxyl group, which is pH-sensitive metal absorber that emits different colors; hence, it is a favorable dye in the textile industry for fabrication purposes. The IUPAC name of alizarin is 1,2-dihydroxyanthracene-9,10-dione with a molecular weight of 220.21 g/mol. Different oxide-based semiconducting nanomaterials can degrade alizarin by the photo-catalytic reaction. The report reveals that alizarin red S was 39% degraded by pure SnO_2 nanoparticles within 120 minutes (Padmaja *et al.*, 2023). Similarly, 91.78 -107 nm size Fe Nps degrades 93.7% alizarin yellow R dye within 42 hours by obeying pseudo-first-order kinetics (Ahmed *et al.*, 2020). The degradation of alizarin red S was obtained at 50% by ZnS NPs and 96.7% by Cd-ZnS in 120 minutes in the irradiation of 300 W/m^2 intensity of light (Jabeen *et al.*, 2017). Furthermore, reports claim that 77% of alizarin was photochemically degraded by ZnO NPs within 90 minutes (Kansal *et al.*, 2013).

The SnO_2/CCAC composite having a size of 17.25 nm with a band gap of 3.52 eV can effectively degrade 90.86% methylene blue within 120 minutes of irradiation of light (Ramamoorthy *et al.*, 2020). Moreover, another finding shows that alizarin yellow was degraded up to 96.4%, alizarin yellow degraded to 87.8%, and aizarin-3-methylamino was 97.3% degraded by CeO_2 doped SnO_2 nanoparticles (Hassan *et al.*, 2020). It was noted that Ti/SnO_2-RuO_2 is efficient in degrading 80.4% alizarin cyanin green at an optimal level while keeping pH 5 at room temperature, results also claimed that 51.3% of the dye is degraded within 40 minutes (S. Chen *et al.*, 2020). In the present work, we have synthesized SnO_2 nanoparticles by the sodium

borohydride reduction method. The obtained nanoparticles were characterized by UV-Visible Spectroscopy, FT-IR, EDX, X-RD, and SEM to analyze photocatalytic efficiency for the degradation of alizarin dye.

Materials and Methods

Materials

Tin chloride ($SnCl_2.2H_2O$, 97%, MW = 225.63 g/mol, BN QF1Q610524) dehydrated purified salt was purchased from Merck company, India. Similarly, sodium borohydride ($NaBH_4$, MW = 37.83 g/mol, CAS No.16940-66-2) was purchased from Merck, India. Polyethylene glycol ($HO(C_2H_4O)n^7H$, MW = 100 g/L, H_2O at 20 °C, CAS No. 25322-68-3) was purchased from Merck, India. Ethanol (C_2H_5OH, >99% purity, MW = 46.06 g/mol, CAS No. 64-17-5) was purchased from Fusion Biotech India. Alizarin ($C_{14}H_8O_4$, MW = 240.21 g/mol, MID = M1513) was purchased from Merck India, and distilled water was obtained from the Nanotechnology lab of RECAST, TU, Nepal.

Methodology

Synthesis of Tin Oxide Nanoparticles (SnO_2 NPs)

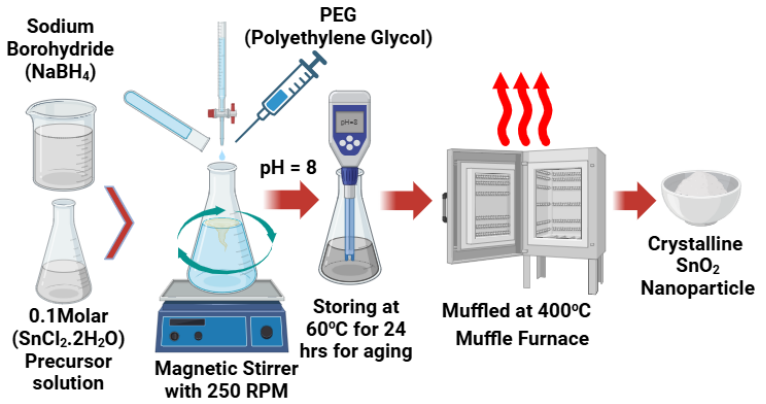

Fig. 1. Synthetic pathway for the preparation of tin oxide nanoparticles (SnO_2 NPs).

A 0.1 M $SnCl_2$ precursor solution was prepared by dissolving 2.2562 gm crystalline $SnCl_2.2H_2O$ salt in 100 ml ethanol. The obtained solution was stirred continuously at room temperature for 1 hour at 90 rpm in a thermoregulatory magnetic stirrer, further; the solution was stirred for 10 minutes at 40°C for complete dissolution to get a clear transparent precursor. The 0.5 M sodium borohydride solution was prepared by dissolving 1.8915 gm in 100 ml deionized distilled water. The precursor was stirred continuously for 1 hour, and then sodium borohydride was added from a burette drop by drop. The pH of the solution was maintained by keeping the pH 8 by adding a low concentration of liquor ammonia in the solution. The stirring was kept continuous for 2 hours by adding polyethylene glycol (PEG) as a capping agent to avoid agglomeration of the reduced mass. The white viscous mass was kept for aging in a hot air oven for 4 hours at 80 °C. The sample was finally kept at 60 °C for 24 hours in the hot air oven for complete evaporation of water, ammonia, and alcohol. Thus, the obtained dry mass was further annealed at 600 °C for 4

hours to get dry crystalline powder of tin oxide nanoparticles which is denoted by SnO_2 NPs in the experiment (Priya *et al.*, 2016; Shahzad *et al.*, 2021; Sun *et al.*, 2004).

Characterization of Tin Oxide Nanoparticles (SnO_2 NPs)

The SnO_2 NPs were characterized by UV-visible double-beam Spectrophotometer (UV-1900i, Shimadzu, Japan). The Fourier Transfer Infra-red (FT-IR, IR Affinity-1s, Shimadzu, Japan) was analyzed to find the stretching and bending of SnO_2 NPs in a specific wavenumber region. Energy Dispersive X-ray (EDX) spectra were analyzed to identify elemental composition (EDX-8000, Shimadzu, Japan). The X-rd. Spectra were analyzed from X-ray Diffractometer (Bruker D2 Phaser, Massachusetts, USA) for the crystallographic texture, size of particles, and crystallinity of the sample.

Photocatalytic activity of SnO_2 NPS

The photocatalytic activity of nanoparticles was observed in atmospheric photo light in August 2024 in the Mid-West University periphery of Surkhet, Nepal, where the intensity of solar radiation was found 5.64±0.14 kWh. The alizarin stock solution was prepared by dissolving 10 mg of anhydrous alizarin powder in 1 liter of deionized distilled water. The photocatalytic degradation was initiated by adding 10 mg SnO_2 NPs to a 100 ml stock solution during exposure to light at different ambient intensities of the day. The photocatalytic process was recorded in the spectrophotometer from starting times to infinite at different wavelengths with their corresponding absorbance. The degradation was also carried out in the dark at different time intervals. The following relation calculated the degradation intensity (Regmi *et al.*, 2015).

$$\% \text{ Efficiency} = \frac{C_{initial} - C_{final}}{C_{initial}} \dots\dots\dots\dots\dots 1$$

Where, $C_{initial}$ = Initial concentration of alizarin, and C_{final} = Final concentration of alizarin at the time ('t' min.). The following equation explains the pseudo-first-order kinetics.

$$-K_t = \ln\frac{C_t}{C_o} \dots\dots\dots\dots\dots 2$$

Where, K_t = Rate constant for pseudo-first-order kinetics. C_t and C_o are the final and initial concentrations of alizarin dye.

Results and Discussion

UV-visible Spectra of SnO_2 NPs

Tin oxide nanoparticles (SnO_2 NPs) show distinct absorbance at 263 nm near the UV region due to their electronic transition from the valence band O_{2p} to the conducting band Sn_{5s} energy state. Based on the wavelength absorption in the plot, the optical band gap obtained from the extrapolation in the Tauc's plot is 3.78 eV, which is quite lower than the band gap of bulk SnO_2, possibly showing the doping/impurity of another element in the particle, and it signifies no quantum confinement. On the flip side of the plot, the band gap of 3.98 eV is also observed with quantum confinement that shows pristine SnO_2 NPs. By solving Brus's equation, we obtained the size of the particle in the range of 3.00 to 4.95 nm diameter. It was reported that the band gap of SnO_2 nanoparticle varies from 3.6 to 4.0, but due to the quantum confinement effect, the band gap was obtained at a higher 3.95 eV than the reported value, probably due to the decreased size of the particle (Koshy *et al.*, 2014).

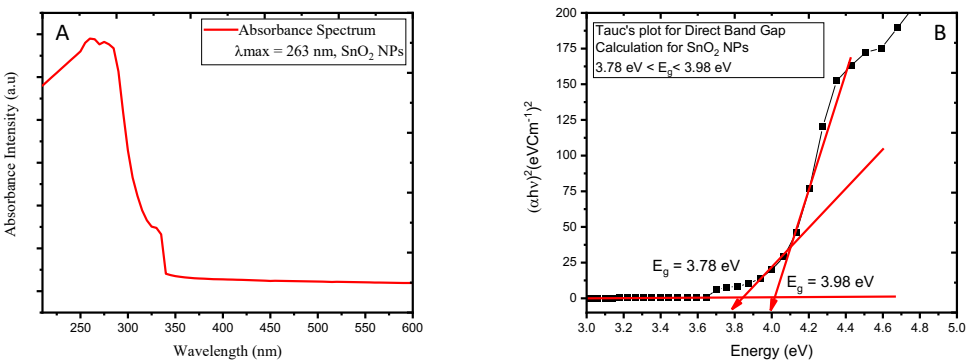

Fig. 2. (A) *UV-visible spectrum of SnO_2 NPs, showing its sharp peak at 263 nm, (B) Tauc's plot for the calculation of the direct band gap of SnO_2 NPs.*

According to Tauc, the optical band gap of the nanoparticle is calculated by the following relations (Tauc *et al.*, 1966).

$$\alpha h\upsilon = A(h\upsilon - Eg)^n \quad \ldots\ldots\ldots\ldots 3$$

The energy hυ(eV), is calculated as;

$$h\upsilon(\text{eV}) = \frac{1240}{\lambda} \ldots\ldots\ldots\ldots 4$$

Where 'α' represents the absorption coefficient, 'h' is Planck's constant 6.626 x 10^{-34} Js, 'υ' represents the frequency of light, E_g represents the optical band gap (eV), 'n' is the constant term which is ½ for direct allowed transition, 2 for indirect allowed transition, 'λ' represents the wavelength in nanometer.

FT-IR Spectra of SnO_2 NPs

FT-IT spectra of SnO_2 NPs show that the sharp O-H stretching observed in 3438.21 cm^{-1} represents the presence of a hydroxyl group due to the absorption of water molecules by the nanoparticle. The stretching and bending of water due to rotation and vibration are sharply observed in 1272.45 cm^{-1} for H-OH bending, and 999.45 cm^{-1} for stretching of the bond between H-O-H. The sharp stretching of Sn-O was observed in 851.91 cm^{-1} and O-Sn-O stretching was observed in 654.81 cm^{-1}. The additional binding and stretching modes in different wavelength regions show the impurities associated with nanoparticles (Altooq *et al.*, 2022; Aziz *et al.*, 2013).

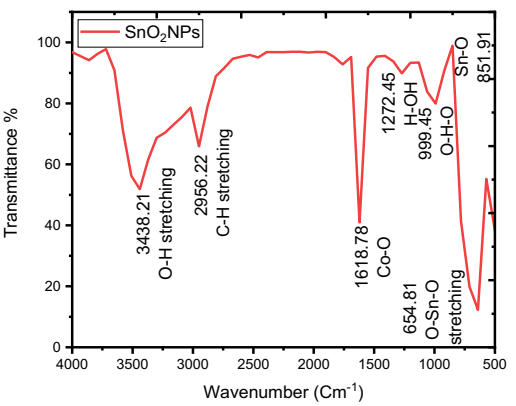

Fig. 3. FT-IR spectra of SnO_2 NPs showing stretching and bending of Sn-O and O-Sn-O at different wavenumber regions.

Elemental Analysis of SnO_2 NPs in EDX

Energy Dispersive X-ray (EDX) analysis reveals that the SnO_2 NPs are mainly composed of tin (Sn) and oxygen (O) atoms. In the detection mode C-Sc up to 12 keV, we haven't analyzed the sharp peak of oxygen atoms. In Al-U mode in EDX-8000, up to 40 keV sharp Oka shows a significant and distinct peak of oxygen with 0.167 keV energy with 13.16% composition in the particle. Furthermore, SnLg1 and SnLg2 peaks are also observed with dispersive energy of 3.81 and 3.88 keV. Similarly, the sharp peak of SnKa, $SnKb_1$, and $SnKb_2$ shows the dispersive energy of 24.2 keV, 28.56, and 29.19 keV respectively. The elemental percentage composition of tin in the sample is found 85.011%. The EDX spectra also reveal a CoKa peak with 5.14 keV with the composition of cobalt (Co) 0.026%, CuKa peak with 6.78 keV and a composition of copper (Cu) 0.043%, and ZnKa with dispersive energy of 8.94 keV with the composition of zinc (Zn) 0.035%. Their insignificant presence in the nanoparticle though decreases the band gap of the particle to some extent, they increase the catalytic efficiency of SnO_2 NPs avoiding the recombination of holes and electrons in the surface (Dhinakar *et al.*, 2016; Kim *et al.*, 2011).

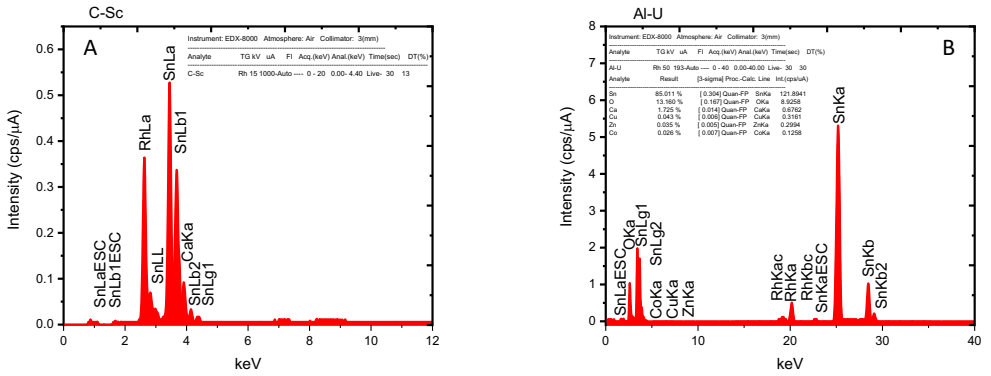

Fig. 4. A. *EDX Analysis of SnO_2 NPs in EDX-8000 for Analyte C-Sc (Rh-15, in 20 keV,1000 uA with DT (%) 13. B. EDX Analysis of SnO_2 NPs in EDX-8000 for Analyte Al-U (Rh-193, in 40 keV,193 uA with DT (%) 30, showing different elemental composition in the particle.*

X-RD Analysis for SnO_2 NPs

X-RD. of SnO_2 NPs reveals the distinct tetragonal rutile geometry with respective indices in 2θ degree having unique diffraction peaks (Aziz *et al.*, 2012; Dias *et al.*, 2020). The miller indices obtained for SnO_2 NPs are 101 (Intensity 1043.6, 2θ = 31.74°), 110 (Intensity 277.78, 2θ = 26.93°), 200 (Intensity 1043.6, 2θ = 33.77°), 211 (Intensity 440.37, 2θ = 45.40°), 220 (Intensity 440.37, 2θ = 45.40°), 002 (Intensity 90.18, 2θ = 56.42°). Furthermore, 301(Intensity 66.03, 2θ = 90.18°), 310 (Intensity 60.93, 2θ = 27.64), 202 (Intensity 69.68, 2θ = 33.89°) and 321 (Intensity 75.04, 2θ = 136.89°) confirms the presence of SnO_2 NPs.

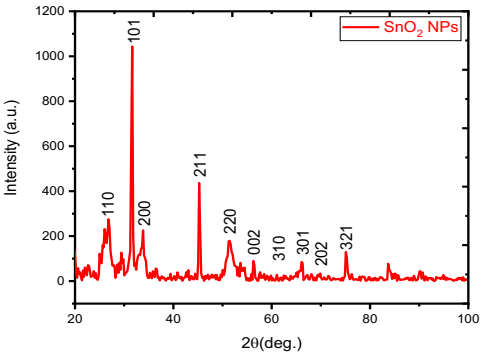

Fig. 5. X-RD. Crystallography of SnO_2 NPs shows different indices in 2-theta degrees with their respective intensity.

The peaks obtained before 2θ = 20° show the lattice distortion in the nanoparticle, which probably increases the amorphous nature of the articles. According to the Debye-Scherrer equation, we have calculated the Full width at half maximum (FWHA)β value for SnO_2 NPs for the peak is 0.2 and λ = 1.5406 Å, source CuKα, k = 0.9 (shape factor), the approximate size of the particle in diameter (D) = 41.28 nm obtained and crystallinity is 43.38% (Holzwarth & Gibson, 2011).

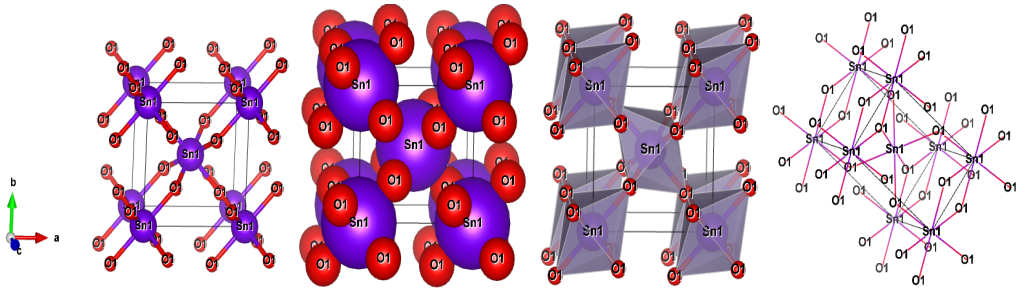

Fig. 6. The 3D structure of SnO_2 depicts Ball and stick, Space-filling, Polyhedral, and Wireframe representation, confirming the crystallography of Tetragonal Rutile geometry (Frazer *et al.*, 2004).

$$D = \frac{K\lambda}{\beta Cos\theta} = \frac{0.9x1.5406}{0.2xCos(15.815)} = 412.84\ Å = 41.28\ nm$$

The crystallinity of SnO_2 NPs was obtained according to the X-rd. Pattern as:

$$\text{Crystallinity} = \frac{\text{Crystalline Area}}{\text{Crystalline Area} + \text{Amorphous Area}} \text{ x } 100\%$$

$$= \frac{5083.762}{5944.50} x100 \approx 85.52\%$$

The synthesized SnO_2 NPs have an average of 41.28 nm diameter and 85.52% crystallinity.

Analysis of light Intensity for Photocatalytic degradation

Photocatalytic degradation of dye occurs because of the absorption of light by SnO_2 NPs having energy equal to its band gap or greater than the band gap that causes exciting electrons from valence to the conducting band; as a result, electron-hole pairs are formed. The mechanism is explained in four fundamental points through the photon absorption by the materials, followed by the generation of reactive free radical species where holes generally oxidize water and electrons reduce oxygen into superoxide radicals. The hydroxide and superoxide radicals are very reactive intermediate chemical species that degrade complex organic molecules into CO_2 and H_2O, ultimately mineralization takes place. In the process, recombining holes and electrons are prevented due to surface modification, either by doping elements that may increase or decrease the catalytic efficiency of SnO_2 NPs (Sapkota *et al.*, 2019, 2020, 2021)

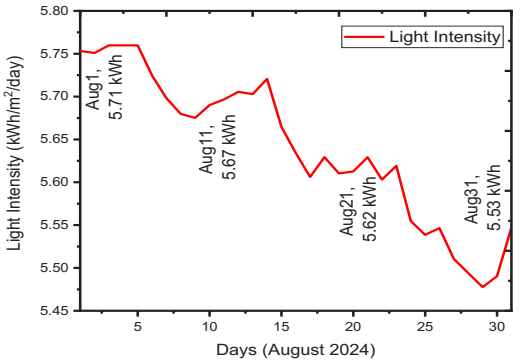

Fig. 7. Light Intensity distribution at Mid-West University, Surkhet, Nepal August 1 to 31, 2024 Photocatalytic degradation of alizarin was accomplished in the application of 5.71 kWh/m^2/day, 5.67 kWh/m^2/day, 5.62 kWh/m^2/day, and 5.53 kWh/m^2/day on different days of August 2024. Variation of intensity in light does not show any kind of enhancement in the degradation process.

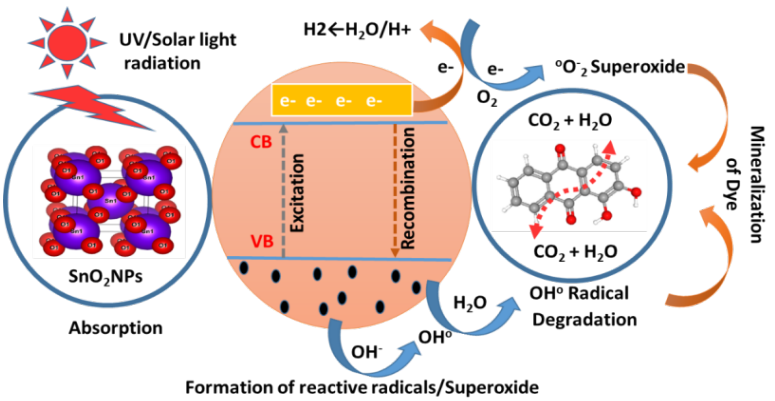

Fig. 8. Schematic diagram showing photocatalytic degradation mechanism of Alizarin on SnO_2 NPs surface.

Photocatalytic Degradation of Alizarin

The experiment was achieved in solar radiation having an intensity of 5.64±0.14 kWh/m^2/day. The process was conducted by adding 10 mg SnO_2 NPs in 100 ml of 10 mg/L alizarin solution in a transparent borosilicate conical flask while maintaining pH 8. The starting point is considered as zero time that was kept in the dark, and the successive experiments were conducted after the 10-minute interval up to the infinite period till the complete degradation of dye was observed. The maximum wavelength absorbed by the alizarin was found at 430.30 nm, and the intensity of absorbance was found to be decreasing up to 110 minutes. The intense red color of alizarin gradually disappeared over an infinite period. After completing the degradation, the entire solution was centrifuged at 5400 rpm, where SnO_2 NPs were settled down in the bottom of the falcon tube. The intact SnO_2 nanoparticles were used again for each successive degradation process. Furthermore, the catalytic degradation was also carried out in the dark for 20-minute intervals of time up to infinite. In the dark, catalytic degradation reduces abruptly. The degradation of dye was found incomplete at an infinite time (Priya *et al.*, 2016; Shahzad *et al.*, 2021; Sun *et al.*, 2004).

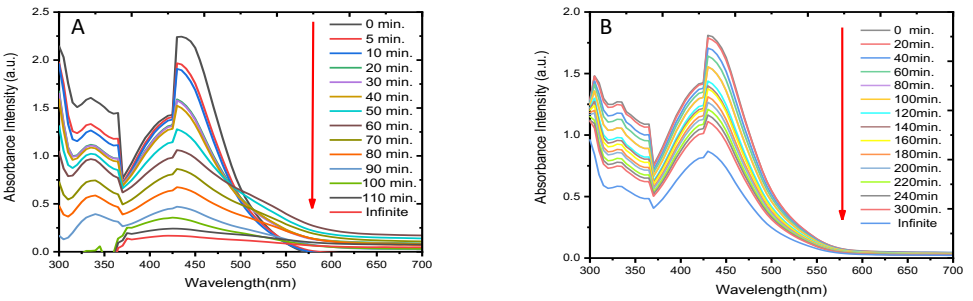

Fig. 9. A. The photocatalytic degradation of alizarin by SnO_2 NPs for an infinite period. B. The catalytic degradation of alizarin in the dark by SnO_2 NPs for an infinite period.

The photo-generated catalysis is explained by the absorption of light by SnO_2 NPs of solar radiation with an energy equal to its band gap or greater than the band gap. The SnO_2 NPs are semiconductors that facilitate the excitation of electrons from the valence band to the conduction band. The jumping of electrons from the particle creates the hole; as a result, electron-hole pairs are formed. The free electron in the conduction band rapidly reacts with the oxygen molecule to form powerful superoxide ($O_2^{\cdot -}$) furthermore, the hole present in the valence band interacts with water molecules/OH^- to form a very reactive $OH^{\cdot}$ radical. The generated reactive free radicals and superoxide degrade the alizarin continuously in the presence of light. Such free radicals can't be generated in the absence of light, but due to the high surface atom in the particle, catalytic degradation occurs slightly. The photocatalytic process is inhibited by the recombination of electron-hole pairs. The catalytic degradation of SnO_2 NPs is explained based on the following reaction steps (Tasisa *et al.*, 2024).

$$SnO_2\ NPs + h\nu \rightarrow h^+_{(VB)} + e^-_{(CB)} \quad \ldots\ldots\ldots 1$$
$$\text{Free } e^-_{(CB)} + O_2 \rightarrow O_2^{\cdot -} \quad \ldots\ldots\ldots 2$$
$$\text{Hole}^+_{(VB)} + H_2O \rightarrow H^+ + OH^{\cdot} \quad \ldots\ldots\ldots 3$$
$$\text{Hole}^+_{(VB)} + OH^- \rightarrow OH^{\cdot} \quad \ldots\ldots\ldots 4$$
$$\text{Alizarin} + OH^{\cdot} \rightarrow CO_2 + H_2O \quad \ldots\ldots\ldots 5$$
$$\text{Alizarin} + O_2^{\cdot -} \rightarrow CO_2 + H_2O \quad \ldots\ldots\ldots 6$$

The catalytic degradation of alizarin by SnO_2 NPs in the dark is probably due to the absorption of dye around the surface of the catalyst. This process can be explained based on electron transfer that ultimately converts water molecules/dissolves oxygen into $OH^{\cdot}/OH^-$ in the solution (Chen & Mao, 2007; Lu *et al.*, 2019).

The kinetics of photocatalytic degradation of SnO_2 NPs was analyzed through pseudo-first-order kinetics. The plot of $\ln(C_t/C_o)$ is plotted against the time taken, giving a straight line with a negative slope -0.02±0.00157. The negative slope is obtained due to the continuous degradation of alizarin with time. The curve was further evaluated by pearson's r, which gives its value -0.96482, and a correlation coefficient of 0.92511 was obtained, approximately equal to 1. The statistical interpretation confirms that the photocatalytic degradation of alizarin by SnO_2 NPs obeys pseudo-order kinetics with a rate constant of 0.02 minute^{-1} and in the dark, the catalytic degradation takes place with a rate constant of 0.00217 minute^{-1}.

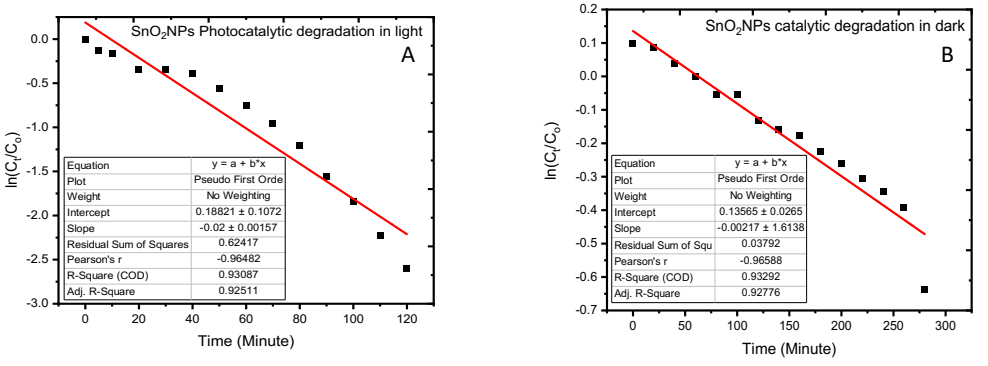

Fig. 10. A. Photocatalytic degradation of alizarin by SnO_2 NPs. B. Catalytic degradation of alizarin by SnO_2 NPs in the dark.

The catalytic degradation of SnO_2 NPs is prolonged in the dark medium. We have potted $\ln(C_t/C_o)$ against time to determine the kinetics plot, but it takes nearly 300 minutes to decompose half of the concentration of alizarin. Though the degradation is prolonged and almost insignificant, it obeys pseudo-first-order kinetics with a negative slope -0.00217±1.6138. The data was further evaluated by pearson's *r* -0.96688, and correlation coefficient *R*-square 0.92776. Photocatalytic degradation of alizarin by SnO_2

NPs obeys pseudo-first-order kinetics better than the catalytic degradation in the dark medium.

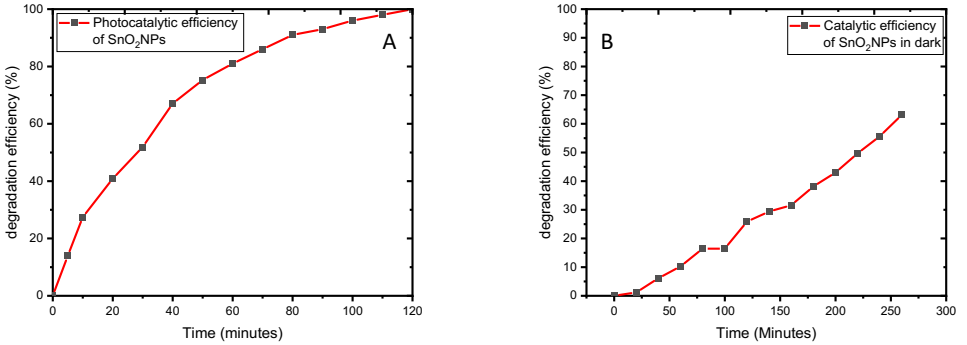

Fig. 11. A. Catalytic efficiency of SnO_2 NPs on alizarin dye in light. B. Catalytic efficiency of SnO_2 NPs on alizarin dye in dark.

The degradation efficiency was calculated and the plot of efficiency against time plots shows that SnO_2 NPs have strong catalytic properties in the light due to absorption, excitation, formation of intermediate superoxide and radicals, and finally recombination mechanism. The plot reveals that the SnO_2 NPs show 100% catalytic efficiency in 120 minutes, but the efficiency becomes prolonged in a dark medium and achieves approximately 68% at the infinite period. The degradation in light and dark depicts that SnO_2 NPs semiconductor materials become efficient with high potential catalysts in the presence of photons but becomes weaker in the dark.

Conclusion

Dyes are toxic organic compounds; slow degradation of dye ultimately causes harmful effects in the body if their concentration is high. In the present work, we synthesized tin oxide nanoparticles using a tin chloride precursor solution using the sodium borohydride reduction method. The obtained SnO_2 nanoparticles were characterized by UV-visible Spectrophotometry, and we obtained their wavelength at 263 nm. The extrapolation of Tauc's plot gave a band gap of 3.78 eV, indicating impurity in the particles. The nanoparticle was further characterized by FT-IR, where sharp stretching of Sn-O was observed in 851.91 cm^{-1} and O-Sn-O stretching was observed in 654.81 cm^{-1}, which confirms the presence of SnO_2 nanoparticles. The Energy Dispersive X-ray (EDX) showed 85.11% tin (Sn), 13.16% oxygen (O), and less than 1% cobalt (Co), copper (Cu), and zinc (Zn) mixture in the nanoparticles. The crystallographic texture of the particles was analyzed through X-rd. that gave 110, 101, 202, 211, and 220 planes that confirm the tetragonal rutile structure of SnO_2 particles. The size of nanoparticles was calculated by the Debye-Scherrer's equation which gave particle size 41.28 ± 14.59 nm with crystallinity 85.52%. The photocatalytic degradation was carried out in the average solar radiation 5.64 ± 0.14 $kWh/m^2/day$ at the optimal wavelength of alizarin 430 nm. The complete degradation for alizarin was obtained in 120 minutes and dark medium degradation was prolonged for up to 300 minutes. The SnO_2 NPs showed 100%

photocatalytic efficiency in the short time frame, but dark medium catalysis was limited to 68%. Tin oxide nanoparticle (SnO_2 NPs) was found efficient in degrading alizarin under controlled pH in the limited time frame.

Acknowledgments

The author would like to thank the RECAST, Tribhuwan University, and Mid-West University, Surkhet for providing laboratory facilities for the research work.

Declaration of Interest

The author declares no competing conflict of interest.

References

Ahmed, A., Usman, M., Yu, B., Ding, X., Peng, Q., Shen, Y., & Cong, H. (2020). Efficient photocatalytic degradation of toxic Alizarin yellow R dye from industrial wastewater using biosynthesized Fe nanoparticle and study of factors affecting the degradationon rate. *Journal of Photochemistry and Photobiology B: Biology*, *202*, 111682. https://doi.org/https://doi.org/10.1016/j.jphotobiol.2019.111682

Alcântara, L. M., Ferreira, T. C. S., Fontana, V., Chatelain, E., Moraes, C. B., & Freitas-Junior, L. H. (2020). A multi-species phenotypic screening assay for leishmaniasis drug discovery shows that active compounds display a high degree of species-specificity. *Molecules*, *25*(11), 2551.

Altooq, N., Humood, A., Alajaimi, A., Alenezi, A. F., Janahi, M., AlHaj, O., & Jahrami, H. (2022). The role of micronutrients in the management of COIVD-19 and optimizing vaccine efficacy. In *Human Nutrition and Metabolism* (Vol. 27). https://doi.org/10.1016/j.hnm.2022.200141

Aziz, M., Abbas, S., & Baharom, W. (2012). Size-controlled synthesis of SnO2 nanoparticles by sol-gel method. *Materials Letters*, *91*, 31–34. https://doi.org/10.1016/j.matlet.2012.09.079

Aziz, M., Abbas, S. S., & Baharom, W. R. W. (2013). Size-controlled synthesis of SnO2 nanoparticles by sol–gel method. *Materials Letters*, *91*, 31–34.

Chen, S., Zhou, L., Yang, T., He, Q., Zhou, P., He, P., Dong, F., Zhang, H., & Jia, B. (2020). Thermal decomposition based fabrication of dimensionally stable Ti/SnO2–RuO2 anode for highly efficient electrocatalytic degradation of alizarin cyanin green. *Chemosphere*, *261*, 128201. https://doi.org/https://doi.org/10.1016/j.chemosphere.2020.128201

Chen, X., & Mao, S. S. (2007). Titanium Dioxide Nanomaterials: Synthesis, Properties, Modifications, and Applications. *Chemical Reviews*, *107*(7), 2891–2959. https://doi.org/10.1021/cr0500535

Daniel, M.-C., & Astruc, D. (2004). Gold nanoparticles: assembly, supramolecular chemistry, quantum-size-related properties, and applications toward biology, catalysis, and nanotechnology. *Chemical Reviews*, *104*(1), 293–346.

Dhinakar, K., Thangaraj, S., Sundar, M., & Bose, A. (2016). Structural, optical and impedance properties of SnO2 nanoparticles. *Journal of Materials Science: Materials in Electronics*, *27*. https://doi.org/10.1007/s10854-016-4497-2

Dias, J. S., Batista, F. R. M., Bacani, R., & Triboni,

E. R. (2020). Structural characterization of SnO nanoparticles synthesized by the hydrothermal and microwave routes. *Scientific Reports*, *10*(1), 9446. https://doi.org/10.1038/s41598-020-66043-4

Din, S. U., Kiani, S. H., Haq, S., Ahmad, P., Khandaker, M. U., Faruque, M. R. I., Idris, A. M., & Sayyed, M. I. (2022). Bio-synthesized tin oxide nanoparticles: Structural, optical, and biological studies. *Crystals*, *12*(5), 614.

Feynman, R. (2018). There's plenty of room at the bottom. In *Feynman and computation* (pp. 63–76). CRC Press.

Frazer, K. A., Pachter, L., Poliakov, A., Rubin, E. M., & Dubchak, I. (2004). VISTA: computational tools for comparative genomics. *Nucleic Acids Research*, *32*(suppl_2), W273–W279.

Hardy, J. A., & Aust, A. E. (1995). Iron in asbestos chemistry and carcinogenicity. *Chemical Reviews*, *95*(1), 97–118.

Hassan, S. S. M., Kamel, A. H., Hassan, A. A., Amr, A. E.-G. E., El-Naby, H. A., & Elsayed, E. A. (2020). A SnO2/CeO2 Nano-Composite Catalyst for Alizarin Dye Removal from Aqueous Solutions. *Nanomaterials*, *10*(2). https://doi.org/10.3390/nano10020254

Holzwarth, U., & Gibson, N. (2011). The Scherrer equation versus the'Debye-Scherrer equation'. *Nature Nanotechnology*, *6*(9), 534.

Jabeen, U., Shah, S. M., & Khan, S. U. (2017). Photo catalytic degradation of Alizarin red S using ZnS and cadmium doped ZnS nanoparticles under unfiltered sunlight. *Surfaces and Interfaces*, *6*, 40–49. https://doi.org/https://doi.org/10.1016/j.surfin.2016.11.002

Kader, M. A., Azmi, N. S., Kafi, A. K. M., Hossain, M. S., Masri, M. F. Bin, Ramli, A. N. M., & Tan, C. S. (2023). Synthesis and Characterization of a Multiporous SnO2 Nanofibers-Supported Au Nanoparticles-Based Amperometric Sensor for the Nonenzymatic Detection of H2O2. *Chemosensors*, *11*(2). https://doi.org/10.3390/chemosensors11020130

Kansal, S. K., Lamba, R., Mehta, S. K., & Umar, A. (2013). Photocatalytic degradation of Alizarin Red S using simply synthesized ZnO nanoparticles. *Materials Letters*, *106*, 385–389. https://doi.org/https://doi.org/10.1016/j.matlet.2013.05.074

Khalilzadeh-Rezaie, F., Oladeji, I., Yusuf, T., Nath, J., Nader, N., Vangala, S., Cleary, J., Schoenfeld, W., & Peale, R. (2015). Optical and electrical properties of tin oxide-based thin films prepared by streaming process for electrodeless electrochemical deposition. *MRS Proceedings*, *1805*. https://doi.org/10.1557/opl.2015.571

Kim, H.-J., Son, J.-H., & Bae, D.-S. (2011). Synthesis and Characterization of SnO2 Nanoparticles by Hydrothermal Processing. *Korean Journal of Materials Research*, *21*. https://doi.org/10.3740/MRSK.2011.21.8.415

Koshy, J., Chandran, A., Samuel, S., & George, K. (2014). *Optical properties of SnO2 nanoparticles*. *1620*, 192–196. https://doi.org/10.1063/1.4898239

Kumar, B., Smita, K., Debut, A., & Cumbal, L. (2020). Synthesis and characterization of SnO2 nanoparticles using cochineal dye. *Applied Physics A*, *126*, 1–9. https://doi.org/10.1007/s00339-020-

03969-6

Lilletvedt, M., Kristensen, S., Tønnesen, H. H., Høgset, A., & Nardo, L. (2010). Time-domain evaluation of drug–solvent interactions of the photosensitizers TPCS2a and TPPS2a as part of physicochemical characterization. *Journal of Photochemistry and Photobiology A: Chemistry*, *214*(1), 40–47.

Lu, C.-C., Hsu, M. H., & Lin, Y.-P. (2019). Evaluation of heavy metal leachability of incinerating recycled aggregate and solidification/stabilization products for construction reuse using TCLP, multi-final pH and EDTA-mediated TCLP leaching tests. *Journal of Hazardous Materials*, *368*, 336–344. https://doi.org/https://doi.org/10.1016/j.jhazmat.2019.01.066

Magnavita, N. (2018). Medical surveillance, continuous health promotion and a participatory intervention in a small company. *International Journal of Environmental Research and Public Health*, *15*(4), 662.

Padmaja, B., Dhanapandian, S., Suthakaran, S., Ashokkumar, K., & Krishnakumar, N. (2023). Hydrothermally developed SnO2 nanoparticles and its photocatalytic degradation of Alizarin red S, Brilliant green and Methyl orange dyes and electrochemical performances. *Inorganic Chemistry Communications*, *149*, 110363. https://doi.org/https://doi.org/10.1016/j.inoche.2022.110363

Priya, M., Geetha, A., & Ramamurthi, K. (2016). Structural, morphological and optical properties of tin oxide nanoparticles synthesized by sol–gel method adding hydrochloric acid. *Journal of Sol-Gel Science and Technology*, *78*. https://doi.org/10.1007/s10971-016-3966-7

Ramamoorthy, M., Ragupathy, S., Sakthi, D., Arun, V., & Kannadasan, N. (2020). Synthesis of SnO2 loaded on corn cob activated carbon for enhancing the photodegradation of methylene blue under sunlight irradiation. *Journal of Environmental Chemical Engineering*, *8*(5), 104331.

Regmi, S., Ghimire, K. N., Pokhrel, M. R., & Khadka, D. B. (2015). Adsorptive removal and recovery of aluminium (III), iron (II), and chromium (VI) onto a low cost functionalized phragmities karka waste. *Journal of Institute of Science and Technology*, *20*(2), 145–152.

Rehan, F., Zhang, M., Fang, J., & Greish, K. (2024). Therapeutic applications of nanomedicine: recent developments and future perspectives. *Molecules*, *29*(9), 2073.

Sahin, O., Stewart, R. A., Faivre, G., Ware, D., Tomlinson, R., & Mackey, B. (2019). Spatial Bayesian Network for predicting sea level rise induced coastal erosion in a small Pacific Island. *Journal of Environmental Management*, *238*, 341–351.

Sapkota, K. P., Lee, I., Hanif, M. A., Islam, M. A., Akter, J., & Hahn, J. R. (2020). Enhanced Visible-Light Photocatalysis of Nanocomposites of Copper Oxide and Single-Walled Carbon Nanotubes for the Degradation of Methylene Blue. *Catalysts*, *10*(3). https://doi.org/10.3390/catal10030297

Sapkota, K. P., Lee, I., Hanif, M. A., Islam, M. A., & Hahn, J. R. (2019). Solar-Light-Driven Efficient ZnO–Single-Walled Carbon Nanotube Photocatalyst for the

Degradation of a Persistent Water Pollutant Organic Dye. *Catalysts*, *9*(6). https://doi.org/10.3390/catal9060498

Sapkota, K. P., Lee, I., Shrestha, S., Islam, A., Hanif, A., Akter, J., & Hahn, J. R. (2021). Coherent CuO-ZnO nanobullets maneuvered for photocatalytic hydrogen generation and degradation of a persistent water pollutant under visible-light illumination. *Journal of Environmental Chemical Engineering*, *9*(6), 106497. https://doi.org/https://doi.org/10.1016/j.jece.2021.106497

Shi, K., Qiu, Y., Li, B., & Stenstrom, M. K. (2016). Effectiveness and potential of straw-and wood-based biochars for adsorption of imidazolium-type ionic liquids. *Ecotoxicology and Environmental Safety*, *130*, 155–162.

Somerville, L., Bareño, J., Jennings, P., McGordon, A., Lyness, C., & Bloom, I. (2016). The effect of pre-analysis washing on the surface film of graphite electrodes. *Electrochimica Acta*, *206*, 70–76.

Stark, W. J., Stoessel, P. R., Wohlleben, W., & Hafner, A. (2015). Industrial applications of nanoparticles. *Chemical Society Reviews*, *44*(16), 5793–5805.

Tasisa, Y. E., Sarma, T. K., Sahu, T. K., & Krishnaraj, R. (2024). Phytosynthesis and characterization of tin-oxide nanoparticles (SnO(2)-NPs) from Croton macrostachyus leaf extract and its application under visible light photocatalytic activities. *Scientific Reports*, *14*(1), 10780. https://doi.org/10.1038/s41598-024-60633-2

Tauc, J., Grigorovici, R., & Vancu, A. (1966). Optical properties and electronic structure of amorphous germanium. *Physica Status Solidi (B)*, *15*(2), 627–637.